

# A Robust Adaptive $\mathcal{H}_\infty$ Controller for Full Flight Envelope of a Convertible UAV

Jonatan M. Campos\* Daniel N. Cardoso\*\* Guilherme V. Raffo\*\*,\*\*

\* Undergraduate Program of Mechanical Engineering, Federal University of Minas Gerais, MG, Brazil (jonatancampos@ufmg.br)

\*\* Graduate Program in Electrical Engineering, Federal University of Minas Gerais, MG, Brazil (danielneri@ufmg.br)

\*\*\* Department of Electronic Engineering, Federal University of Minas Gerais, MG, Brazil (raffo@ufmg.br)

---

**Abstract:** A Tilt-Rotor Unmanned Aerial Vehicle (UAV) is an underactuated mechanical system with highly nonlinear and coupled dynamics, that is often subjected to parametric uncertainties, unmodeled dynamics, and external disturbances. To cope with such adversities, this work proposes a robust adaptive controller capable of handling the full flight envelope of the UAV which is composed of cruise and hover flight modes. Most importantly, this work addresses the transition between hover and cruise flight and vice versa. To do so, a multi-body nonlinear dynamic model of a Quad-tiltrotor Convertible Plane (CP) Vertical Take-Off and Landing (VTOL) UAV, here called QuadCP-VTOL, is obtained using the Lagrangian formalism which takes into account nonconservative forces and torques applied by the propellers, tilting mechanisms, canards, wings, and horizontal stabilizers. Thereafter, a Linear Parameter Varying (LPV) model that covers the full flight envelope of the aircraft is derived from the nonlinear model. Accordingly to the adaptive mixing technique, several robust  $\mathcal{H}_\infty$  state feedback controllers are designed based on a parallel distribution compensation (PDC) method alongside a pole clustering technique to ensure better closed-loop performance. Results of numerical experiments conducted on a high fidelity simulator in a Hardware in the Loop (HIL) framework are presented to corroborate the efficacy of the proposed control strategy.

*Keywords:* Robust Adaptive Control; Convertible Tilt-Rotor UAV; Parallel Distributed Compensation

---

## 1. INTRODUCTION

Unmanned Aerial Vehicles (UAVs) have been widely investigated in the last decades. Whereas a few years ago the research on UAVs have been mostly conducted in a few laboratories and at early operational stages in the military domain (Ducard and Allenspach, 2021), nowadays the interest in developing such systems has increased. Several configurations of UAVs, such as fixed and rotary wings, have been proposed to comply with a broad range of applications, such as surveillance, load transportation, and search and rescue missions. Among the UAV configurations, the Tilt-Rotor stands out for its capabilities of performing vertical take-off and landing (VTOL), as rotary wing UAVs, and cruise flight with higher speeds and endurance, as fixed wing UAVs, providing better energy consumption and overall flight performance. Moreover, its four rotor variant improves the maneuverability at lower speeds and allows generating larger yaw torques by differentiating the angular velocity of the propellers (Allenspach and Ducard, 2021).

---

\* This work was supported by the Brazilian agencies CNPq, CAPES, FAPEMIG, and FAPESP. The authors would also like to acknowledge the INCT (National Institute of Science and Technology) for Cooperative Autonomous Systems Applied to Security and Environment under the grant CNPq 465755/2014-3, FAPESP 2014/50851-0.

Regarding the control of Tilt-Rotor UAVs, the large dynamic variation between flight modes poses an interesting challenge on the control design. Whereas in helicopter-flight mode (hover and VTOL) the deflection of the aerodynamic control surfaces (aileron, rudder, elevator) produces neglectable dynamical effects, in airplane flight mode small deflections produce significant aerodynamic forces that can be used to generate both the necessary forces to sustain forward flight and the moments that allow control and guidance. This dynamic behavior prevents the design of controllers using simple linear control techniques to handle all flight modes of Tilt-Rotor UAVs. In this context, aiming to simplify the control problem, several works deal only with the helicopter-flight mode, as, for example, Lombaerts et al. (2019) that design a controller using nonlinear dynamic inversion, and Vendrichoski et al. (2019) that design a simple linear controller with the goal to evaluate the system when performing tasks that require interaction with the environment.

The works that address the full flight envelope trajectory tracking are usually based on gain scheduling techniques and, although satisfactory results are obtained, they do not ensure stability. The lack of stability guarantees is evidenced in works such as Hegde et al. (2021), where multiple PID controllers are used for different flight modes and

a mode switching algorithm is used to schedule the controllers. The adaptive PID is compared with a robust  $\mathcal{H}_\infty$  controller under the presence of disturbances, parametric uncertainties and noise. Numerical experiments covering the full flight envelope of the aircraft are presented where, through the Integral of Absolute Error (IAE) index, is possible to observe that the  $\mathcal{H}_\infty$  controller outperforms the adaptive PID controller. Authors in Houari et al. (2020) have also proposed a comparison between controllers for a tri-tilt rotor configuration. In that case, Fuzzy Logic is employed to perform an intelligent scheduling of candidate controllers. Candidate PID controllers are compared with candidate LQR ones, evidencing the poor performance of the former. Although satisfactory results are achieved, the designed LQR lacks in disturbance rejection, often required for this kind of system. A similar approach is also found in Willis et al. (2020).

In this context, this paper presents the mathematical modeling of a QuadCP-VTOL UAV and proposes a Robust Adaptive Mixing Controller (RAMC) with candidate controllers designed through a Parallel Distributed Compensation (PDC) formulation. The controller is able to ensure stability while handling the trajectory tracking throughout the full flight envelope of the QuadCP-VTOL UAV. In order to design the controller, an LPV model that represents the full flight envelope of the QuadCP-VTOL UAV is obtained from the nonlinear model considering the forward velocity's magnitude as a varying parameter. Based on this model, several candidate controllers are designed through the linear  $\mathcal{H}_\infty$  control strategy. The adaptive mixing scheme, proposed in Cardoso et al. (2021), is reformulated to perform a convex combination of the candidate controllers with ensured stability. In order to improve the performance and reduce conservatism of the controllers proposed in our previous work (Campos et al., 2021), here linear  $\mathcal{H}_\infty$  candidate controllers are designed considering a PDC approach and a parameter varying Lyapunov function. Additionally, the proposed controller is validated in a high fidelity simulator developed based on ROS and Gazebo through a Hardware-In-the-Loop (HIL) simulation. With this simulation valuable insights regarding the fulfillment of real time constraints and resource consumption of the embedded system can be obtained. Moreover, the control system can be evaluated when performing dangerous or hard tasks with reduced cost, risks and time consumption when compared with tests in the physical prototype.

## 2. QUADCP-VTOL UAV MODELING

The QuadCP-VTOL UAV is a multi-body mechanical system composed of five rigid bodies: the main body, which comprehends the fuselage, canards, and wings; and four groups of thrusters, two at each side of the aircraft, with each one being composed of a propeller, a rotor, and a tilting mechanism. Figure 1 shows the aircraft details. Notice that the rear groups of thrusters include the vertical stabilizers, that rotate together with the rear tilting mechanisms.

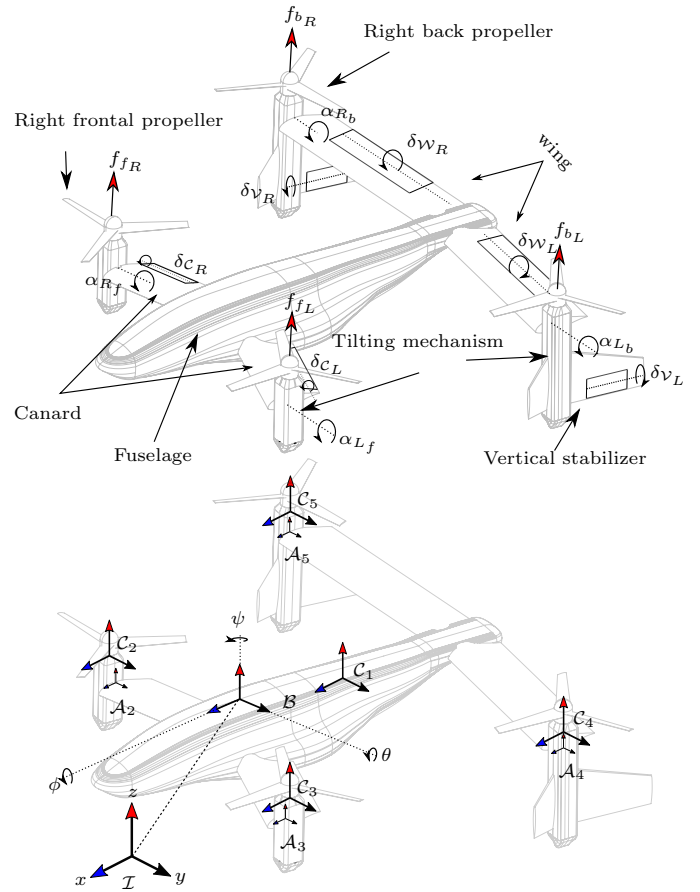


Figure 1. The QuadCP-VTOL UAV and the rigidly attached coordinate systems to obtain the kinematic model.

### 2.1 Kinematic Model

To obtain the forward kinematics, eleven frames are rigidly attached to the system, as illustrated in Figure 1, which are: the inertial reference frame  $\mathcal{I}$ , the body reference frame  $\mathcal{B}$ , the frames attached to center of mass of the main body  $\mathcal{C}_1$  and to the center of mass of each group of thruster,  $\mathcal{C}_2, \mathcal{C}_3, \mathcal{C}_4$  and  $\mathcal{C}_5$ , and the auxiliary frames  $\mathcal{A}_2, \mathcal{A}_3, \mathcal{A}_4, \mathcal{A}_5$ , which are located at the axes of rotation of the tilting mechanisms.

Regarding these frames, the position of the center of mass of the five rigid bodies are computed as<sup>1</sup>

$$\mathbf{p}_{\mathcal{C}_1}^{\mathcal{I}} = \mathbf{R}_{\mathcal{B}}^{\mathcal{I}} \mathbf{d}_{\mathcal{C}_1}^{\mathcal{B}} + \boldsymbol{\xi}, \quad (1)$$

$$\mathbf{p}_{\mathcal{C}_i}^{\mathcal{I}} = \mathbf{R}_{\mathcal{A}_i}^{\mathcal{I}} \mathbf{d}_{\mathcal{C}_i}^{\mathcal{A}_i} + \mathbf{R}_{\mathcal{B}}^{\mathcal{I}} \mathbf{d}_{\mathcal{A}_i}^{\mathcal{B}} + \boldsymbol{\xi}, \quad (2)$$

for  $i \in \{2, 3, 4, 5\}$ , where  $\boldsymbol{\xi} \triangleq [x \ y \ z]^T$  is the position of the origin of  $\mathcal{B}$  with respect to  $\mathcal{I}$ , and  $\mathbf{d}_{\mathcal{C}_1}^{\mathcal{B}}, \mathbf{d}_{\mathcal{A}_i}^{\mathcal{B}}, \mathbf{d}_{\mathcal{C}_i}^{\mathcal{A}_i} \in \mathbb{R}^3$  are constant vectors that represent the displacement between the origins of the subscripts and superscripts frames. Besides,  $\mathbf{R}_{\mathcal{B}}^{\mathcal{I}} \in \text{SO}(3)$  is a rotation matrix, with  $\mathbf{R}_{\mathcal{B}}^{\mathcal{I}} \triangleq \mathbf{R}_{z,\psi} \mathbf{R}_{y,\theta} \mathbf{R}_{x,\phi}$ , in which  $\phi, \theta$ , and  $\psi$  are Euler angles, with the ZYX convention about the local axes, which describe the orientation of  $\mathcal{B}$  with respect to  $\mathcal{I}$ , and  $\mathbf{R}_{\mathcal{A}_i}^{\mathcal{I}} \in \text{SO}(3)$  is defined as  $\mathbf{R}_{\mathcal{A}_i}^{\mathcal{I}} \triangleq \mathbf{R}_{\mathcal{B}}^{\mathcal{I}} \mathbf{R}_{\mathcal{A}_i}^{\mathcal{B}}$ , with  $\mathbf{R}_{\mathcal{A}_2}^{\mathcal{B}} = \mathbf{R}_{y,\alpha_{Rf}} \mathbf{R}_{x,-\beta}$ ,  $\mathbf{R}_{\mathcal{A}_3}^{\mathcal{B}} = \mathbf{R}_{y,\alpha_{Lf}} \mathbf{R}_{x,\beta}$ ,

<sup>1</sup> For the sake of simplicity, throughout the manuscript, some function dependencies are omitted.

$\mathbf{R}_{A_4}^B = \mathbf{R}_{y,\alpha_{L_b}} \mathbf{R}_{x,-\beta}$ , and  $\mathbf{R}_{A_5}^B = \mathbf{R}_{y,\alpha_{R_b}} \mathbf{R}_{x,\beta}$ , where  $\alpha_{R_f}$ ,  $\alpha_{L_f}$ ,  $\alpha_{R_b}$ , and  $\alpha_{L_b}$  are the tilting angles of the frontal right and left, and rear right and left tilting mechanisms, respectively. Besides,  $\beta \in \mathbb{R}_{\geq 0}$  is a small inclination angle of the propellers towards the fuselage, which is introduced to increase the system controllability (Raffo et al., 2011).

From (1) and (2), the linear velocities of the centers of mass of the five rigid bodies are computed as

$$\mathbf{v}_{C_j}^{\mathcal{I}} = \dot{\mathbf{p}}_{C_j}^{\mathcal{I}} = \mathbf{J}_{C_j} \dot{\mathbf{q}}, \quad (3)$$

for  $j \in \{1, 2, 3, 4, 5\}$ , where  $\mathbf{q} \triangleq [\xi' \ \eta' \ \alpha']'$  is the vector of generalized coordinates, with  $\eta \triangleq [\phi \ \theta \ \psi]'$ ,  $\alpha \triangleq [\alpha_{R_f} \ \alpha_{L_f} \ \alpha_{L_b} \ \alpha_{R_b}]'$ , and  $\mathbf{J}_{C_j} = \partial \mathbf{p}_{C_j}^{\mathcal{I}} / \partial \mathbf{q}$ . In addition, the angular velocities of the five rigid bodies are given by

$$\boldsymbol{\omega}_{C_j}^{\mathcal{I}} = \mathbf{W}_{C_j} \dot{\mathbf{q}}, \quad (4)$$

with  $\mathbf{W}_{C_j} \triangleq \partial \boldsymbol{\omega}_{C_j}^{\mathcal{I}} / \partial \dot{\mathbf{q}}$ , in which  $\boldsymbol{\omega}_{C_1}^{\mathcal{I}} = \mathbf{R}_B^{\mathcal{I}} \mathbf{W} \eta \dot{\eta}$ ,  $\boldsymbol{\omega}_{C_2}^{\mathcal{I}} = \mathbf{R}_{A_4}^{\mathcal{I}} \mathbf{W} \eta \dot{\eta} + \mathbf{R}_{C_2}^{\mathcal{I}} \mathbf{a}_{y_R} \alpha_{R_f}$ ,  $\boldsymbol{\omega}_{C_3}^{\mathcal{I}} = \mathbf{R}_B^{\mathcal{I}} \mathbf{W} \eta \dot{\eta} + \mathbf{R}_{C_3}^{\mathcal{I}} \mathbf{a}_{y_L} \alpha_{L_f}$ ,  $\boldsymbol{\omega}_{C_4}^{\mathcal{I}} = \mathbf{R}_{A_5}^{\mathcal{I}} \mathbf{W} \eta \dot{\eta} + \mathbf{R}_{C_4}^{\mathcal{I}} \mathbf{a}_{y_L} \alpha_{L_b}$ ,  $\boldsymbol{\omega}_{C_5}^{\mathcal{I}} = \mathbf{R}_B^{\mathcal{I}} \mathbf{W} \eta \dot{\eta} + \mathbf{R}_{C_5}^{\mathcal{I}} \mathbf{a}_{y_R} \alpha_{R_b}$ , where  $\mathbf{W} \eta \triangleq \begin{bmatrix} 1 & 0 & -\sin \theta \\ 0 & \cos \phi & \sin \phi \cos \theta \\ 0 & -\sin \phi & \cos \phi \cos \theta \end{bmatrix}$ ,  $\mathbf{a}_{y_R} \triangleq (\mathbf{R}_{x,-\beta})' \mathbf{a}_y$ ,  $\mathbf{a}_{y_L} \triangleq (\mathbf{R}_{x,\beta})' \mathbf{a}_y$ ,  $\mathbf{a}_y \triangleq [0 \ 1 \ 0]'$ , and  $\mathbf{R}_{C_j}^{\mathcal{I}} = \mathbf{R}_{A_j}^{\mathcal{I}}$ .

## 2.2 Equations of Motion

The equations of motion of the QuadCP-VTOL UAV are written in the Euler-Lagrange canonical form

$$\mathbf{M}(\mathbf{q}) \ddot{\mathbf{q}} + \mathbf{C}(\mathbf{q}, \dot{\mathbf{q}}) \dot{\mathbf{q}} + \mathbf{g}(\mathbf{q}) = \boldsymbol{\vartheta}(\dot{\mathbf{q}}, \mathbf{q}, \mathbf{u}, \boldsymbol{\zeta}), \quad (5)$$

where  $\mathbf{M}(\mathbf{q}) \in \mathbb{R}^{10 \times 10}$  is the inertia matrix,  $\mathbf{C}(\mathbf{q}, \dot{\mathbf{q}}) \in \mathbb{R}^{10 \times 10}$  is the Coriolis and centripetal force matrix,  $\mathbf{g}(\mathbf{q}) \in \mathbb{R}^{10}$  is the gravitational force vector, and  $\boldsymbol{\vartheta}(\dot{\mathbf{q}}, \mathbf{q}, \mathbf{u}, \boldsymbol{\zeta}) \in \mathbb{R}^{10}$  is the vector of generalized forces, in which  $\mathbf{u} \in \mathbb{R}^{11}$  and  $\boldsymbol{\zeta} \in \mathbb{R}^3$  are, respectively, the control input and disturbance vectors.

The inertia matrix is obtained through the total kinetic energy of the system, which is given by

$$\begin{aligned} \mathcal{K} &= \sum_{j=1}^5 \frac{1}{2} \dot{\mathbf{q}}' (m_{C_j} (\mathbf{J}_{C_j})' \mathbf{J}_{C_j} + (\mathbf{W}_{C_j})' \mathbf{R}_{C_j}^{\mathcal{I}} \mathbb{I}_{C_j} (\mathbf{R}_{C_j}^{\mathcal{I}})' \mathbf{W}_{C_j}) \dot{\mathbf{q}} \\ &= \frac{1}{2} \dot{\mathbf{q}}' \mathbf{M}(\mathbf{q}) \dot{\mathbf{q}}, \end{aligned} \quad (6)$$

where  $m_{C_j} \in \mathbb{R}$  and  $\mathbb{I}_{C_j} \in \mathbb{R}^{3 \times 3}$  are the mass and the inertia tensor matrix, with respect to its own coordinate frame, of the  $j$ -th body, respectively. The Coriolis and centripetal force matrix is obtained from the inertia matrix through the Christoffel symbols of first kind. Additionally, the gravitational force vector is computed as  $\mathbf{g}(\mathbf{q}) = \partial \mathcal{P} / \partial \mathbf{q}$ , with  $\mathcal{P} \triangleq -\sum_{j=1}^5 m_{C_j} \mathbf{g}_r' \mathbf{p}_{C_j}^{\mathcal{I}}$  being the total potential energy of the system, where  $\mathbf{g}_r \triangleq [0 \ 0 \ -9.8]'$  ( $m/s^2$ ).

The generalized force vector,  $\boldsymbol{\vartheta}(\dot{\mathbf{q}}, \mathbf{q}, \mathbf{u}, \boldsymbol{\zeta})$ , is composed of nonconservative forces and torques that actuate in the QuadCP-VTOL UAV. Here, this vector is divided into six components,  $\boldsymbol{\vartheta}(\dot{\mathbf{q}}, \mathbf{q}, \mathbf{u}, \boldsymbol{\zeta}) = \boldsymbol{\vartheta}_{\mathcal{P}} + \boldsymbol{\vartheta}_S + \boldsymbol{\vartheta}_{\mathcal{F}} + \boldsymbol{\vartheta}_C + \boldsymbol{\vartheta}_{\mathcal{W}} + \boldsymbol{\vartheta}_{\mathcal{V}}$ , where  $\boldsymbol{\vartheta}_{\mathcal{P}}$ ,  $\boldsymbol{\vartheta}_S$ ,  $\boldsymbol{\vartheta}_{\mathcal{F}}$ ,  $\boldsymbol{\vartheta}_C$ ,  $\boldsymbol{\vartheta}_{\mathcal{W}}$ , and  $\boldsymbol{\vartheta}_{\mathcal{V}}$  are generated by the propellers, tilting mechanisms, fuselage, canards, wings, and vertical stabilizers, respectively. Besides, the generalized force vector is a function of the control input vector  $\mathbf{u} \triangleq [f_{f_R} \ f_{f_L} \ f_{b_L} \ f_{b_R} \ \tau_{f_R} \ \tau_{f_L} \ \tau_{b_L} \ \tau_{b_R} \ \delta_C \ \delta_{\mathcal{W}} \ \delta_{\mathcal{V}}]'$ , in

<sup>2</sup> Throughout the manuscript the subscripts  $R$  and  $L$  are used to distinguish between the right and left sides of the aircraft, and the subscripts  $f$  and  $b$  means the front and back sides.

which  $f_{f_R}$ ,  $f_{f_L}$ ,  $f_{b_L}$ , and  $f_{b_R}$  are the applied propeller forces,  $\tau_{f_R}$ ,  $\tau_{f_L}$ ,  $\tau_{b_L}$ , and  $\tau_{b_R}$  are the applied tilting mechanism torques,  $\delta_C = \delta_{C_R} = \delta_{C_L}$  are the canard control surface deflections,  $\delta_{\mathcal{W}} = -\delta_{\mathcal{W}_R} = \delta_{\mathcal{W}_L}$  are the aileron deflections, and  $\delta_{\mathcal{V}} = \delta_{\mathcal{V}_R} = \delta_{\mathcal{V}_L}$  are the rudder deflections. Also, the generalized force vector is a function of the disturbance vector  $\boldsymbol{\zeta} = [u_a \ v_a \ w_a]'$ , here described by the environment wind speed expressed in  $\mathcal{I}$ .

The propellers' contribution to the generalized forces are computed as

$$\begin{aligned} \boldsymbol{\vartheta}_{\mathcal{P}} &= \left[ (\mathbf{J}_{C_2})' + (\mathbf{W}_{C_2})' \frac{k_{\tau}}{b} \lambda_{f_R} \right] \mathbf{R}_{C_2}^{\mathcal{I}} \mathbf{a}_z f_{f_R} \\ &+ \left[ (\mathbf{J}_{C_3})' + (\mathbf{W}_{C_3})' \frac{k_{\tau}}{b} \lambda_{f_L} \right] \mathbf{R}_{C_3}^{\mathcal{I}} \mathbf{a}_z f_{f_L} \\ &+ \left[ (\mathbf{J}_{C_4})' + (\mathbf{W}_{C_4})' \frac{k_{\tau}}{b} \lambda_{b_L} \right] \mathbf{R}_{C_4}^{\mathcal{I}} \mathbf{a}_z f_{b_L} \\ &+ \left[ (\mathbf{J}_{C_5})' + (\mathbf{W}_{C_5})' \frac{k_{\tau}}{b} \lambda_{b_R} \right] \mathbf{R}_{C_5}^{\mathcal{I}} \mathbf{a}_z f_{b_R}, \end{aligned} \quad (7)$$

where  $\mathbf{a}_z \triangleq [0 \ 0 \ 1]'$ , and the terms  $k_{\tau} \in \mathbb{R}$  and  $b \in \mathbb{R}$  are the drag and thrust constants of the propellers that must be estimated. Besides,  $\lambda_{\hat{n}} \in \{-1, 1\}$  is given according to the direction of rotation of the corresponding propeller.

The vector of generalized forces generated by the tilting mechanisms is given by

$$\begin{aligned} \boldsymbol{\vartheta}_S &= [\mathbf{W}_{C_2} - \mathbf{W}_{C_1}]' \mathbf{R}_{C_2}^{\mathcal{I}} \mathbf{a}_y \tau_{f_R} + [\mathbf{W}_{C_3} - \mathbf{W}_{C_1}]' \mathbf{R}_{C_3}^{\mathcal{I}} \mathbf{a}_y \tau_{f_L} \\ &+ [\mathbf{W}_{C_4} - \mathbf{W}_{C_1}]' \mathbf{R}_{C_4}^{\mathcal{I}} \mathbf{a}_y \tau_{b_L} + [\mathbf{W}_{C_5} - \mathbf{W}_{C_1}]' \mathbf{R}_{C_5}^{\mathcal{I}} \mathbf{a}_y \tau_{b_R} \\ &- \begin{bmatrix} \mathbf{0}_{6 \times 6} & \mathbf{0}_{6 \times 4} \\ \mathbf{0}_{4 \times 6} & \mathbf{I}_{4 \times 4} \end{bmatrix} \dot{\mathbf{q}}, \end{aligned} \quad (8)$$

where  $v \in \mathbb{R}$  is the tilting mechanism friction coefficient.

To compute the aerodynamic forces, the UAV is divided into seven aerodynamic surfaces. Then, seven frames are rigidly attached to the aerodynamic center of each aerodynamic surface, which are given by  $\mathcal{A} \in \{\mathcal{F}, \mathcal{C}_R, \mathcal{C}_L, \mathcal{W}_R, \mathcal{W}_L, \mathcal{V}_R, \mathcal{V}_L\}$ , where  $\mathcal{F}$  denotes fuselage,  $\mathcal{C}_R$  and  $\mathcal{C}_L$  denote the right and left canards,  $\mathcal{W}_R$  and  $\mathcal{W}_L$  denote the right and left wings, and  $\mathcal{V}_R$  and  $\mathcal{V}_L$  denote the right and left vertical stabilizers.

It is assumed each aerodynamic center position as a fixed point within the respective aerodynamic surface. The position of the aerodynamic centers of the fuselage, canards, and wings are given by

$$\mathbf{p}_{\mathcal{N}}^{\mathcal{I}} = \mathbf{R}_B^{\mathcal{I}} \mathbf{d}_{\mathcal{N}}^{\mathcal{B}} + \boldsymbol{\xi}, \quad (9)$$

for  $\mathcal{N} \in \{\mathcal{F}, \mathcal{C}_R, \mathcal{C}_L, \mathcal{W}_R, \mathcal{W}_L\}$ , where  $\mathbf{d}_{\mathcal{N}}^{\mathcal{B}} \in \mathbb{R}^3$  is the distance between  $\mathcal{B}$  and the aerodynamic center  $\mathcal{N}$ , which remains constant. In addition, the positions of the aerodynamic centers of the vertical stabilizers vary according to the inclination of the rear tilting mechanisms as follows

$$\mathbf{p}_{\mathcal{V}_L}^{\mathcal{I}} = \mathbf{R}_B^{\mathcal{I}} \mathbf{R}_{A_4}^{\mathcal{B}} \mathbf{d}_{\mathcal{V}_L}^{A_4} + \mathbf{R}_B^{\mathcal{I}} \mathbf{d}_{A_4}^{\mathcal{B}} + \boldsymbol{\xi}, \quad (10)$$

$$\mathbf{p}_{\mathcal{V}_R}^{\mathcal{I}} = \mathbf{R}_B^{\mathcal{I}} \mathbf{R}_{A_5}^{\mathcal{B}} \mathbf{d}_{\mathcal{V}_R}^{A_5} + \mathbf{R}_B^{\mathcal{I}} \mathbf{d}_{A_5}^{\mathcal{B}} + \boldsymbol{\xi}, \quad (11)$$

where  $\mathbf{d}_{\mathcal{V}_L}^{A_4}$ ,  $\mathbf{d}_{\mathcal{V}_R}^{A_5} \in \mathbb{R}^3$  are the positions of  $\mathcal{V}_L$  and  $\mathcal{V}_R$  with respect to  $A_4$  and  $A_5$ , respectively. Accordingly, the velocities of the aerodynamic centers,  $\mathbf{v}_{\mathcal{A}}^{\mathcal{I}}$ , are computed by taking the time derivative of (9)-(11), and expressed as  $\mathbf{v}_{\mathcal{A}}^{\mathcal{I}} = \mathbf{J}_{\mathcal{A}} \dot{\mathbf{q}}$ , with  $\mathbf{J}_{\mathcal{A}} \triangleq \partial \mathbf{p}_{\mathcal{A}}^{\mathcal{I}} / \partial \mathbf{q}$ .

The magnitudes of the relative wind speed actuating at the aerodynamic centers, in the  $\mathbf{x}$ - $\mathbf{y}$  and  $\mathbf{x}$ - $\mathbf{z}$  planes, are computed, respectively, by  $v_{\mathcal{A}xz}^{air} = \sqrt{(w^A)^2 + (u^A)^2}$ , and  $v_{\mathcal{A}xy}^{air} = \sqrt{(v^A)^2 + (u^A)^2}$ , where  $[u^A \ v^A \ w^A]' = (\mathbf{R}_{\mathcal{A}}^{\mathcal{I}})' (\mathbf{v}_{\mathcal{A}}^{\mathcal{I}} - \boldsymbol{\zeta})$ ,

with  $\mathbf{R}_{\mathcal{F}}^{\mathcal{I}} = \mathbf{R}_{\mathcal{C}_R}^{\mathcal{I}} = \mathbf{R}_{\mathcal{C}_L}^{\mathcal{I}} = \mathbf{R}_{\mathcal{B}}^{\mathcal{I}}$ ,  $\mathbf{R}_{\mathcal{W}_R}^{\mathcal{I}} \triangleq \mathbf{R}_{\mathcal{B}}^{\mathcal{I}} \mathbf{R}_{x,-\epsilon}$ , and  $\mathbf{R}_{\mathcal{W}_L}^{\mathcal{I}} = \mathbf{R}_{\mathcal{B}}^{\mathcal{I}} \mathbf{R}_{x,\epsilon}$ ,  $\mathbf{R}_{\mathcal{V}_R}^{\mathcal{I}} = \mathbf{R}_{\mathcal{C}_4}^{\mathcal{I}} \mathbf{R}_{y,-\frac{\pi}{2}}$  and  $\mathbf{R}_{\mathcal{V}_L}^{\mathcal{I}} = \mathbf{R}_{\mathcal{C}_5}^{\mathcal{I}} \mathbf{R}_{y,-\frac{\pi}{2}}$ , in which  $\epsilon \in \mathbb{R}$  is the dihedral angle of the wings. Therefore, the aerodynamic pressure that actuates on the aerodynamic centers in the  $\mathbf{x}$ - $\mathbf{y}$  and  $\mathbf{x}$ - $\mathbf{z}$  planes of  $\mathcal{A}$  are given, respectively, by  $\kappa_{\mathcal{A}_{xz}}^{air} = \frac{1}{2} \rho (v_{\mathcal{A}_{xz}}^{air})^2$ , and  $\kappa_{\mathcal{A}_{xy}}^{air} = \frac{1}{2} \rho (v_{\mathcal{A}_{xy}}^{air})^2$ , where  $\rho \in \mathbb{R}$  is the air density. The orientation of the relative wind speed is written in terms of the angle of attack and the side slip angle<sup>3</sup> that are computed, respectively, by  $\alpha_{\mathcal{A}}^{air} = \text{atan}(w^A/u^A)$ , and  $\beta_{\mathcal{A}}^{air} = \text{atan}(v^A/u^A)$ .

The lift, drag and side forces generated due to the relative wind speed that actuates on the fuselage can be obtained by

$$f_{\mathcal{F}_{xz}}^d = -\kappa_{\mathcal{F}_{xz}}^{air} s_{\mathcal{F}_{xz}} c_{\mathcal{F}_{xz}}^d(\alpha_{\mathcal{F}}^{air}), \quad (12)$$

$$f_{\mathcal{F}_{xz}}^l = \kappa_{\mathcal{F}_{xz}}^{air} s_{\mathcal{F}_{xz}} c_{\mathcal{F}_{xz}}^l(\alpha_{\mathcal{F}}^{air}), \quad (13)$$

$$f_{\mathcal{F}_{xy}}^d = -\kappa_{\mathcal{F}_{xy}}^{air} s_{\mathcal{F}_{xy}} c_{\mathcal{F}_{xy}}^d(\beta_{\mathcal{F}}^{air}), \quad (14)$$

$$f_{\mathcal{F}_{xy}}^y = \kappa_{\mathcal{F}_{xy}}^{air} s_{\mathcal{F}_{xy}} c_{\mathcal{F}_{xy}}^y(\beta_{\mathcal{F}}^{air}), \quad (15)$$

where  $c_{\mathcal{F}_{xz}}^d(\alpha_{\mathcal{F}}^{air})$  and  $c_{\mathcal{F}}^l(\alpha_{\mathcal{F}}^{air})$  are coefficients of lift and drag forces of the fuselage, from the perspective of the angle of attack, and  $c_{\mathcal{F}_{xy}}^d(\beta_{\mathcal{F}}^{air})$  and  $c_{\mathcal{F}_{xy}}^y(\beta_{\mathcal{F}}^{air})$  are coefficients of drag and side forces, from the perspective of the side slip angle. It is assumed that these coefficients are adimensionalized with respect to the surface areas  $s_{\mathcal{F}_{xz}}$  and  $s_{\mathcal{F}_{xy}}$ . Considering (12)-(15), the vector of generalized forces generated by the fuselage is given by

$$\boldsymbol{\vartheta}_{\mathcal{F}} = (\mathbf{J}_{\mathcal{F}})' \mathbf{R}_{\mathcal{F}}^{\mathcal{I}} \left( \mathbf{R}_{\alpha_{\mathcal{F}}^{air}}^{\mathcal{F}} \begin{bmatrix} f_{\mathcal{F}_{xz}}^d \\ 0 \\ f_{\mathcal{F}_{xz}}^l \end{bmatrix} + \mathbf{R}_{\beta_{\mathcal{F}}^{air}}^{\mathcal{F}} \begin{bmatrix} f_{\mathcal{F}_{xy}}^d \\ f_{\mathcal{F}_{xy}}^y \\ 0 \end{bmatrix} \right), \quad (16)$$

where the matrices  $\mathbf{R}_{\alpha_{\mathcal{F}}^{air}}^{\mathcal{F}} \triangleq \mathbf{R}_{y,-\alpha_{\mathcal{F}}^{air}}$  and  $\mathbf{R}_{\beta_{\mathcal{F}}^{air}}^{\mathcal{F}} \triangleq \mathbf{R}_{z,-\beta_{\mathcal{F}}^{air}}$  are used to express the drag, lift and side forces from the relative wind speed orientation to frame  $\mathcal{F}$ .

The aerodynamic forces generated by the right and left canards as well as the forces generated by the right and left wings can be computed for  $\mathcal{S} \in \{\mathcal{C}, \mathcal{W}\}$  as

$$f_{\mathcal{S}_{R_{xz}}}^d = -\kappa_{\mathcal{S}_{R_{xz}}}^{air} s_{\mathcal{S}} c_{\mathcal{S}}^d(\alpha_{\mathcal{S}_R}^{air}), \quad (17)$$

$$f_{\mathcal{S}_{R_{xz}}}^l = \kappa_{\mathcal{S}_{R_{xz}}}^{air} s_{\mathcal{S}} \left[ c_{\mathcal{S}}^l(\alpha_{\mathcal{S}_R}^{air}) + c^{\delta_S} \delta_{\mathcal{S}_R} \right], \quad (18)$$

$$f_{\mathcal{S}_{L_{xz}}}^d = -\kappa_{\mathcal{S}_{L_{xz}}}^{air} s_{\mathcal{S}} c_{\mathcal{S}}^d(\alpha_{\mathcal{S}_L}^{air}), \quad (19)$$

$$f_{\mathcal{S}_{L_{xz}}}^l = \kappa_{\mathcal{S}_{L_{xz}}}^{air} s_{\mathcal{S}} \left[ c_{\mathcal{S}}^l(\alpha_{\mathcal{S}_L}^{air}) + c^{\delta_S} \delta_{\mathcal{S}_L} \right], \quad (20)$$

where  $c_{\mathcal{S}_i}^d(\alpha_{\mathcal{S}_i}^{air})$  and  $c_{\mathcal{S}_i}^l(\alpha_{\mathcal{S}_i}^{air})$  with  $i \in \{R, L\}$  are the drag and lift coefficients of the canards or wings, from the perspective of its angle of attack, and  $c^{\delta_S}$  is an adimensional control stability derivative associated to the deflection of the canard or wing control surface. It is assumed that these coefficients are adimensionalized with respect to the surface area  $s_{\mathcal{S}}$ .

Considering (17)-(20), the contributions of the canards and wings to the generalized forces vector are computed, respectively, by

$$\boldsymbol{\vartheta}_{\mathcal{C}} = (\mathbf{J}_{\mathcal{C}_R})' \mathbf{R}_{\mathcal{C}_R}^{\mathcal{I}} \mathbf{R}_{\alpha_{\mathcal{C}_R}^{air}}^{\mathcal{C}_R} \begin{bmatrix} f_{\mathcal{C}_{R_{xz}}}^d \\ 0 \\ f_{\mathcal{C}_{R_{xz}}}^l \end{bmatrix} + (\mathbf{J}_{\mathcal{C}_L})' \mathbf{R}_{\mathcal{C}_L}^{\mathcal{I}} \mathbf{R}_{\alpha_{\mathcal{C}_L}^{air}}^{\mathcal{C}_L} \begin{bmatrix} f_{\mathcal{C}_{L_{xz}}}^d \\ 0 \\ f_{\mathcal{C}_{L_{xz}}}^l \end{bmatrix},$$

<sup>3</sup> The angle of attack and the side slip angle are obtained according to the frames rigidly attached to the aerodynamic centers of each aerodynamic surface. They do not follow the aerodynamic convention "NED".

$$\boldsymbol{\vartheta}_{\mathcal{W}} = (\mathbf{J}_{\mathcal{W}_R})' \mathbf{R}_{\mathcal{W}_R}^{\mathcal{I}} \mathbf{R}_{\alpha_{\mathcal{W}_R}^{air}}^{\mathcal{W}_R} \begin{bmatrix} f_{\mathcal{W}_R}^d \\ 0 \\ f_{\mathcal{W}_R}^l \end{bmatrix} + (\mathbf{J}_{\mathcal{W}_L})' \mathbf{R}_{\mathcal{W}_L}^{\mathcal{I}} \mathbf{R}_{\alpha_{\mathcal{W}_L}^{air}}^{\mathcal{W}_L} \begin{bmatrix} f_{\mathcal{W}_L}^d \\ 0 \\ f_{\mathcal{W}_L}^l \end{bmatrix},$$

where  $\mathbf{R}_{\alpha_{\mathcal{C}_R}^{air}}^{\mathcal{C}_R} = \mathbf{R}_{y,-\alpha_{\mathcal{C}_R}^{air}}$ ,  $\mathbf{R}_{\alpha_{\mathcal{C}_L}^{air}}^{\mathcal{C}_L} = \mathbf{R}_{y,-\alpha_{\mathcal{C}_L}^{air}}$ ,  $\mathbf{R}_{\alpha_{\mathcal{W}_R}^{air}}^{\mathcal{W}_R} = \mathbf{R}_{y,-\alpha_{\mathcal{W}_R}^{air}}$ , and  $\mathbf{R}_{\alpha_{\mathcal{W}_L}^{air}}^{\mathcal{W}_L} = \mathbf{R}_{y,-\alpha_{\mathcal{W}_L}^{air}}$ .

The drag and side forces generated by the vertical stabilizers are given by

$$f_{\mathcal{V}_{R_{xy}}}^d = -\kappa_{\mathcal{V}_{R_{xy}}}^{air} s_{\mathcal{V}} c_{\mathcal{V}}^d(\beta_{\mathcal{V}_R}^{air}), \quad (21)$$

$$f_{\mathcal{V}_{R_{xy}}}^y = \kappa_{\mathcal{V}_{R_{xy}}}^{air} s_{\mathcal{V}} \left[ c_{\mathcal{V}}^y(\beta_{\mathcal{V}_R}^{air}) + c^{\delta_{\mathcal{V}}} \delta_{\mathcal{V}_R} \right], \quad (22)$$

$$f_{\mathcal{V}_{L_{xy}}}^d = -\kappa_{\mathcal{V}_{L_{xy}}}^{air} s_{\mathcal{V}} c_{\mathcal{V}}^d(\beta_{\mathcal{V}_L}^{air}), \quad (23)$$

$$f_{\mathcal{V}_{L_{xy}}}^y = \kappa_{\mathcal{V}_{L_{xy}}}^{air} s_{\mathcal{V}} \left[ c_{\mathcal{V}}^y(\beta_{\mathcal{V}_L}^{air}) + c^{\delta_{\mathcal{V}}} \delta_{\mathcal{V}_L} \right], \quad (24)$$

where  $c_{\mathcal{V}_i}^d(\beta_{\mathcal{V}_i}^{air})$  and  $c_{\mathcal{V}_i}^y(\beta_{\mathcal{V}_i}^{air})$  with  $i \in \{R, L\}$  are coefficients of drag and side forces of the horizontal stabilizers, from the perspective of its side slip angle, and  $c^{\delta_{\mathcal{V}}}$  is an adimensional control stability derivative associated to the rudder deflection. It is assumed adimensionalized coefficients with respect to the surface area  $s_{\mathcal{V}}$ . Consequently, the contributions of the vertical stabilizers to the generalized force vector are obtained as

$$\boldsymbol{\vartheta}_{\mathcal{H}} = \mathbf{J}'_{\mathcal{V}_R} \mathbf{R}_{\mathcal{V}_R}^{\mathcal{I}} \begin{bmatrix} f_{\mathcal{V}_{R_{xy}}}^d \\ f_{\mathcal{V}_{R_{xy}}}^y \\ 0 \end{bmatrix} + \mathbf{J}'_{\mathcal{V}_L} \mathbf{R}_{\mathcal{V}_L}^{\mathcal{I}} \begin{bmatrix} f_{\mathcal{V}_{L_{xy}}}^d \\ f_{\mathcal{V}_{L_{xy}}}^y \\ 0 \end{bmatrix}. \quad (25)$$

### 3. LPV MODEL

The adaptive mixing control law, proposed in the following, mixes the candidate controllers based on the QuadCP-VTOL UAV forward motion. Therefore, in order to express the UAV forward velocity,  $u_b$ , as a state of the system, the following mapping between the generalized velocities and the body linear velocities is performed:

$$\dot{\mathbf{q}} = \begin{bmatrix} \mathbf{R}_{\mathcal{B}}^{\mathcal{I}} & 0 & 0 \\ 0 & \mathbf{W}_{\eta}^{-1} & 0 \\ 0 & 0 & \mathbf{I}_4 \end{bmatrix} \dot{\mathbf{q}} = \boldsymbol{\Lambda} \dot{\mathbf{q}}, \quad (26)$$

where  $\dot{\mathbf{q}} \triangleq [u_b \ v_b \ w_b \ p \ q \ r \ \alpha_{R_f} \ \alpha_{L_f} \ \alpha_{L_b} \ \alpha_{R_b}]'$ . From (26), one obtains  $\dot{\mathbf{q}} = \boldsymbol{\Lambda} \dot{\mathbf{q}} + \boldsymbol{\Lambda} \dot{\mathbf{q}}$ . Replacing the latter in (5), the equations of motion are written as  $\boldsymbol{\Lambda} \dot{\mathbf{q}} + \boldsymbol{\Lambda} \dot{\mathbf{q}} = \mathbf{M}(\mathbf{q})^{-1} [\boldsymbol{\vartheta} - \mathbf{g}(\mathbf{q}) - \mathbf{C}(\mathbf{q}, \boldsymbol{\Lambda} \dot{\mathbf{q}}) \boldsymbol{\Lambda} \dot{\mathbf{q}}]$ , yielding the state space representation

$$\begin{bmatrix} \dot{\mathbf{q}} \\ \dot{\mathbf{q}} \end{bmatrix} = \begin{bmatrix} \boldsymbol{\Lambda} \dot{\mathbf{q}} \\ \boldsymbol{\Lambda}^{-1} [-\boldsymbol{\Lambda} \dot{\mathbf{q}} + \mathbf{M}(\mathbf{q})^{-1} \boldsymbol{\Xi}] \end{bmatrix}, \quad (27)$$

with  $\boldsymbol{\Xi} \triangleq \boldsymbol{\vartheta} - \mathbf{g}(\mathbf{q}) - \mathbf{C}(\mathbf{q}, \boldsymbol{\Lambda} \dot{\mathbf{q}}) \boldsymbol{\Lambda} \dot{\mathbf{q}}$ .

Since the generalized coordinates  $x$ ,  $y$ , and  $z$  are external variables for the QuadCP-VTOL UAV dynamic model (27) (i.e. they do not shape the inertia matrix and, consequently, the Coriolis matrix), the system can be separated into two interconnected subsystems related to: i) the planar motion; and ii) the altitude and attitude motions. The planar motion is controlled in an outer-loop through a kinematic nonlinear controller (see Cardoso et al. (2021) for details), which generates the desired linear velocities to be used as a reference by the inner-loop controller.

Accordingly, the nonlinear model (27) is partitioned, and the inner-loop controller is designed taking into account the reduced state vector  $\tilde{\mathbf{x}} = [\tilde{\mathbf{q}}' \ \tilde{\mathbf{q}}']'$ , with  $\tilde{\mathbf{q}} = [z \ \phi \ \theta \ \psi \ \alpha_{R_f} \ \alpha_{L_f} \ \alpha_{L_b} \ \alpha_{R_b}]'$ , yielding

$$\dot{\tilde{\mathbf{x}}} = \mathbf{h}(\tilde{\mathbf{x}}, \mathbf{u}, \boldsymbol{\zeta}). \quad (28)$$

The inner-loop controller is designed based on the RAMC, for which, initially, system (28) is linearized through the first order Taylor series expansion around a generic trajectory  $(\tilde{\mathbf{x}}_{tr}, \mathbf{u}_{tr}, \boldsymbol{\zeta}_{tr})$ , assuming  $\boldsymbol{\zeta}_{tr} = \mathbf{0}_{3 \times 1}$ , yielding

$$\Delta \dot{\tilde{\mathbf{x}}} = \tilde{\mathbf{A}}(\boldsymbol{\epsilon}) \Delta \tilde{\mathbf{x}} + \tilde{\mathbf{B}}_u(\boldsymbol{\epsilon}) \Delta \mathbf{u} + \tilde{\mathbf{B}}_\zeta(\boldsymbol{\epsilon}) \Delta \boldsymbol{\zeta}, \quad (29)$$

where  $\Delta(\cdot) \triangleq (\cdot) - (\cdot)_{tr}$ , in which “tr” denotes desired trajectory,  $\tilde{\mathbf{A}}(\boldsymbol{\epsilon}) \in \mathbb{R}^{18 \times 18}$ ,  $\tilde{\mathbf{B}}_u(\boldsymbol{\epsilon}) \in \mathbb{R}^{18 \times 14}$ ,  $\tilde{\mathbf{B}}_\zeta(\boldsymbol{\epsilon}) \in \mathbb{R}^{18 \times 3}$ , and  $\boldsymbol{\epsilon} = [\tilde{\mathbf{x}}_{tr}, \mathbf{u}_{tr}]$ . In addition, the state-space equation (29) is augmented with integral actions of the regulated states according to the new state vector  $\Delta \mathbf{x} = [\Delta \tilde{\mathbf{q}}' \Delta \tilde{\mathbf{q}}' \int \Delta z \int \Delta u \int \Delta v \int \Delta \psi]'$ , resulting in

$$\Delta \dot{\mathbf{x}} = \mathbf{A}(\boldsymbol{\epsilon}) \Delta \mathbf{x} + \mathbf{B}_u(\boldsymbol{\epsilon}) \Delta \mathbf{u} + \mathbf{B}_\zeta(\boldsymbol{\epsilon}) \Delta \boldsymbol{\zeta}. \quad (30)$$

To comply with the control objective enunciated at the beginning of this section, the inner-loop controller must handle a generic desired trajectory given by  $\tilde{\mathbf{x}}_{tr} = [z_{tr} \ \mathbf{0}_{1 \times 2} \ \psi_{tr} \ \alpha_{R_{f_{tr}}} \ \alpha_{L_{f_{tr}}} \ \alpha_{L_{b_{tr}}} \ \alpha_{R_{b_{tr}}} \ u_{b_{tr}} \ \mathbf{0}_{1 \times 9}]'$  and  $\mathbf{u}_{tr} = [f_{f_{R_{tr}}} \ f_{f_{L_{tr}}} \ f_{b_{L_{tr}}} \ f_{b_{R_{tr}}} \ \tau_{f_{R_{tr}}} \ \tau_{f_{L_{tr}}} \ \tau_{b_{L_{tr}}} \ \tau_{b_{R_{tr}}} \ \mathbf{0}_{1 \times 3}]'$ . This trajectory leads to  $\boldsymbol{\epsilon} = [\alpha_{R_{f_{tr}}} \ \alpha_{L_{f_{tr}}} \ \alpha_{L_{b_{tr}}} \ \alpha_{R_{b_{tr}}} \ u_{b_{tr}} \ f_{f_{R_{tr}}} \ f_{f_{L_{tr}}} \ f_{b_{L_{tr}}} \ f_{b_{R_{tr}}} \ \tau_{f_{R_{tr}}} \ \tau_{f_{L_{tr}}} \ \tau_{b_{L_{tr}}} \ \tau_{b_{R_{tr}}}]$  in (30). Of note, all the variables in  $\boldsymbol{\epsilon}$  are correlated with the forward velocity  $u_{b_{tr}}$ . Therefore, taking into account the set

$$\Omega \triangleq \{u_{b_{tr}} : 0 \leq u_{b_{tr}} \leq u_{b_{tr}}^{max}\}, \quad (31)$$

the system (28) is trimmed considering several equidistant forward velocity values  $u_{b_{tr}}^{(j)} \in \Omega$ , with  $u_{b_{tr}}^{(j+1)} - u_{b_{tr}}^{(j)} = \varrho_u$ , and  $\varrho_u \in \mathbb{R}$ , in order to generate the trimming points  $(\tilde{\mathbf{x}}_{tr}^{(j)}, \mathbf{u}_{tr}^{(j)})$ , for  $j \in \{1, 2, \dots, n_j\}$ . Additionally, (30) is evaluated at each trimming point  $(\tilde{\mathbf{x}}_{tr}^{(j)}, \mathbf{u}_{tr}^{(j)})$  in order to produce an array of linear state space models which are interpolated using a weighting function to produce the LPV system (Baranyi, 2004)

$$\Delta \dot{\mathbf{x}} = \sum_{j=1}^{n_j} \delta^{(j)}(u_{b_{tr}}) \left( \mathbf{A}^{(j)} \Delta \mathbf{x} + \mathbf{B}_u^{(j)} \Delta \mathbf{u} + \mathbf{B}_\zeta^{(j)} \Delta \boldsymbol{\zeta} \right), \quad (32)$$

where matrices  $\mathbf{A}^{(j)}$ ,  $\mathbf{B}_u^{(j)}$ , and  $\mathbf{B}_\zeta^{(j)}$  are called vertex systems. The term  $\delta^{(j)}(u_{b_{tr}})$ , for  $j \in \{1, \dots, n_j\}$ , is a weighting function that performs a convex combination of the vertex systems according to the forward velocity  $u_{b_{tr}}$ . The weighting function must satisfy  $\delta^{(j)}(u_{b_{tr}}) \geq 0$  and  $\sum_{j=1}^{n_j} \delta^{(j)}(u_{b_{tr}}) = 1$ , for any  $u_{b_{tr}} \in \Omega$ .

#### 4. ROBUST ADAPTIVE MIXING CONTROL DESIGN

The RAMC designed in this work takes into account system (32) and consists of two main components: (i) the candidate controllers; and (ii) the mixing scheme. The control objective is to obtain a control input  $\Delta \mathbf{u}$  so that the states  $\Delta \mathbf{x}$  converges to zero for any  $u_{b_{tr}} \in \Omega$ .

In order to generate the RAMC, the set  $\Omega$  is split into several subsets  ${}^{(r)}\Omega \triangleq \{u_{b_{tr}} : {}^{(r)}u_{b_{tr}}^{min} \leq u_{b_{tr}} \leq {}^{(r)}u_{b_{tr}}^{max}\}$ , for  $r \in \{1, 2 \dots n_r\}$ , in which  ${}^{(r)}u_{b_{tr}}^{min}, {}^{(r)}u_{b_{tr}}^{max} \in \mathbb{R}$  are, respectively, the minimum and maximum values of the set  ${}^{(r)}\Omega$ , such that the following properties are satisfied: P1)  $\Omega = {}^{(1)}\Omega \cup {}^{(2)}\Omega \cup \dots \cup {}^{(n_r)}\Omega$ , P2)  ${}^{(r)}\Omega \cap {}^{(r+1)}\Omega \neq \emptyset$ , P3)  ${}^{(r)}\Omega \cap {}^{(r+2)}\Omega = \emptyset$ . In each subset  ${}^{(r)}\Omega$ , system (32) is represented by

$$\Delta \dot{\mathbf{x}} = \sum_k \delta^{(k)}(u_{b_{tr}}) \left( \mathbf{A}^{(k)} \Delta \mathbf{x} + \mathbf{B}_u^{(k)} \Delta \mathbf{u} + \mathbf{B}_\zeta^{(k)} \Delta \boldsymbol{\zeta} \right), \quad (33)$$

for all  $k$  such that  $u_{b_{tr}}^{(k)} \in {}^{(r)}\Omega$ .

Then, to design each candidate controller, system (33) is represented in the following form:

$$\mathcal{P} : \begin{cases} \Delta \dot{\mathbf{x}} = \mathbf{A}^{(r)}(\delta) \Delta \mathbf{x} + \mathbf{B}_u^{(r)}(\delta) \Delta \mathbf{u} + \mathbf{B}_w^{(r)}(\delta) \Delta \mathbf{w}, \\ z = \mathbf{C}_z \Delta \mathbf{x} + \mathbf{D}_{uz} \Delta \mathbf{u} + \mathbf{D}_{wz} \Delta \mathbf{w}, \\ \Delta \mathbf{u} = \mathbf{K}^{(r)}(\delta) \Delta \mathbf{x}, \end{cases} \quad (34)$$

where  $\mathbf{A}^{(r)}(\delta) \triangleq \sum_k \delta^{(k)}(u_{b_{tr}}) \mathbf{A}^{(k)}$ ,  $\mathbf{B}_u^{(r)}(\delta) \triangleq \sum_k \delta^{(k)}(u_{b_{tr}}) \mathbf{B}_u^{(k)}$ ,  $\mathbf{B}_w^{(r)}(\delta) \triangleq \sum_k \delta^{(k)}(u_{b_{tr}}) \mathbf{B}_w^{(k)}$ , for all  $k$  such that  $u_{b_{tr}}^{(k)} \in {}^{(r)}\Omega$ . Moreover,  $\mathbf{B}_w^{(k)} \triangleq [\mathbf{B}_\zeta^{(k)} \ \mathbf{B}_w]$  and  $\Delta \mathbf{w}(t) \triangleq [\Delta \boldsymbol{\zeta}'(t) \ \delta_w'(t)]'$ , in which  $\delta_w(t) \in \mathbb{R}^{10}$  represents the total effects generated by unmodeled dynamics and parametric uncertainties, and  $\mathbf{B}_w = [\mathbf{0}'_{8 \times 10} \ \mathbf{I}'_{10} \ \mathbf{0}'_{4 \times 10}]'$ . Besides,  $\mathbf{K}^{(r)}(\delta) \triangleq \sum_k \delta^{(k)}(u_{b_{tr}}) \mathbf{K}^{(k)}$  is the feedback gain, and  $z(t)$  is the cost variable weighted by the matrices  $\mathbf{C}_z$ ,  $\mathbf{D}_{uz}$  and  $\mathbf{D}_{wz}$ , which are tuned according to the control objectives.

#### 4.1 Linear $\mathcal{H}_\infty$ Candidate Controllers

For each subset  ${}^{(r)}\Omega$ , a candidate PDC state feedback controller

$$\Delta \mathbf{u}^{(r)} = \mathbf{K}^{(r)}(\delta) \Delta \mathbf{x} \quad (35)$$

is designed offline to meet the control requirements. In order to provide attenuation of unknown exogenous disturbances to the closed-loop system, the candidate controllers are designed through the linear  $\mathcal{H}_\infty$  control approach.

The linear  $\mathcal{H}_\infty$  control problem is stated as

$$\min \gamma, \text{ s.t.} \\ \dot{\mathbf{V}}^{(r)}(\delta) + \frac{1}{\gamma} \mathbf{z}(t)' \mathbf{z}(t) - \gamma \Delta \mathbf{w}(t)' \Delta \mathbf{w}(t) < 0, \quad (36)$$

with a quadratic parameter varying Lyapunov function  $\mathbf{V}^{(r)}(\delta) = \Delta \mathbf{x}(t)' (\mathbf{P}^{(r)}(\delta))^{-1} \Delta \mathbf{x}(t)$ .

With some manipulations, the inequality (36) becomes,

$$\hat{\mathbf{x}}(t)' \left( \begin{bmatrix} \mathbf{0} & \mathbf{P}^{(r)}(\delta) & \mathbf{0} \\ * & \mathbf{0} & \mathbf{0} \\ * & * & -\gamma \mathbf{I} \end{bmatrix} + \frac{1}{\gamma} \Phi_1' \Phi_1 \right) \hat{\mathbf{x}}(t) < 0, \quad (37)$$

where  $\hat{\mathbf{x}}(t)' = [\Delta \mathbf{x}(t)' \ \Delta \hat{\mathbf{x}}(t)' \ \Delta \mathbf{w}(t)']$  and  $\Phi_1 = [\tilde{\mathbf{C}}^{(r)} \ \mathbf{0} \ \mathbf{D}_{wz}]$  with  $\tilde{\mathbf{C}}^{(r)} = \mathbf{C}'_z + \mathbf{K}^{(r)}(\delta)' \mathbf{D}_{uz}$ .

In addition, with some manipulations to the first equality in (34), we obtain

$$[\mathbf{A}^{(r)}(\delta) + \mathbf{B}_u^{(r)}(\delta) \mathbf{K}^{(r)}(\delta) - \mathbf{I} \ \mathbf{B}_w^{(r)}(\delta)] \hat{\mathbf{x}}(t) = 0. \quad (38)$$

Now we recall Finsler's Lemma, which is employed here in order to introduce slack variables into the optimization problem (36).

*Lemma 1.* (De Oliveira and Skelton (2001)). Let  $\mathbf{y} \in \mathbb{R}^{n_y}$  and  $\mathcal{B} \in \mathbb{R}^{n_b \times n_y}$ , with  $n_b < n_y$ . Therefore, the following statements are equivalent:

$$\exists \mathcal{Q} \in \mathbb{R}^{n_y \times n_y} : \mathbf{y}' \mathcal{Q} \mathbf{y} < 0, \ \mathcal{B} \mathbf{y} = 0, \ \forall \mathbf{y} \neq 0, \quad (39)$$

$$\exists \mathcal{Q} \in \mathbb{R}^{n_y \times n_y} : (\mathcal{B}^\perp)' \mathcal{Q} \mathcal{B}^\perp < 0, \quad (40)$$

$$\exists \mathcal{Q} \in \mathbb{R}^{n_y \times n_y}, \exists \epsilon \in \mathbb{R} : \mathcal{Q} - \epsilon \mathcal{B}' \mathcal{B} < 0, \quad (41)$$

$$\exists \mathcal{Q} \in \mathbb{R}^{n_y \times n_y}, \exists \mathcal{X} \in \mathbb{R}^{n_y \times n_b} : \mathcal{Q} + \mathcal{X} \mathcal{B} + \mathcal{B}' \mathcal{X}' < 0. \quad (42)$$

Therefore, regarding (37) and (38), the equivalences between (39) and (42), considering  $\mathcal{X}^{(r)} \triangleq [\boldsymbol{\chi}^{(r)} \ \mu \boldsymbol{\chi}^{(r)} \ \mathbf{0}]$  where  $\mu$  is an a priori provided scalar, and applying

the linearizing transformations  $\mathcal{Z}_{(r)} \triangleq (\mathcal{X}_{(r)}^{-1})'$ ,  $\mathcal{Y}_{(r)}(\delta) \triangleq \mathbf{K}_{(r)}(\delta)\mathcal{Z}_{(r)}$ ,  $\tilde{\mathbf{P}}_{(r)}(\delta) \triangleq \mathcal{Z}'_{(r)}(\mathbf{P}_{(r)})^{-1}(\delta)\mathcal{Z}_{(r)}$ , one obtains

$$\begin{bmatrix} \Psi_1^{(r)} & \Psi_2^{(r)} & B_{w(r)}(\delta) \\ * & -\mu(\mathcal{Z} + \mathcal{Z}') & \mu B_{w(r)}(\delta) \\ * & * & -\gamma \mathbf{I} \end{bmatrix} + \frac{1}{\gamma} \begin{bmatrix} \tilde{\mathbf{C}}'_{(r)} \\ \mathbf{0} \\ \mathbf{D}'_{wz} \end{bmatrix} [\tilde{\mathbf{C}}'_{(r)} \quad \mathbf{0} \quad \mathbf{D}'_{wz}] < 0, \quad (43)$$

where  $\tilde{\mathbf{C}}'_{(r)} \triangleq \mathcal{Z}'_{(r)}\mathbf{C}'_z + \mathcal{Y}_{(r)}(\delta)'\mathbf{D}'_{uz}$ ,  $\Psi_1^{(r)} \triangleq \mathbf{A}^{(r)}(\delta)\mathcal{Z}_{(r)} + \mathcal{Z}'_{(r)}\mathbf{A}^{(r)}(\delta) + \mathbf{B}_u^{(r)}(\delta)\mathcal{Y}_{(r)}(\delta) + \mathcal{Y}_{(r)}(\delta)'\mathbf{B}_u^{(r)}(\delta)$ . Then, using the inequality (De Oliveira et al., 2002)

$$(\mathcal{Z}_{(r)})'(\mathbf{P}^{(r)}(\delta))^{-1}\mathcal{Z}_{(r)} > (\mathcal{Z}_{(r)})' + \mathcal{Z}_{(r)} - \mathbf{P}^{(r)}(\delta), \quad (44)$$

we have  $\Psi_2^{(r)} \triangleq \mathcal{Z}_{(r)} + \mathcal{Z}'_{(r)} - \mathbf{P}^{(r)}(\delta) + \mu(\mathcal{Z}'\mathbf{A}^{(r)}(\delta)' + \mathcal{Y}_{(r)}(\delta)'\mathbf{B}_u^{(r)}(\delta)')$ . Finally, by applying Schur's complement to (43), the following expression is obtained

$$\Psi^{(r)} = \begin{bmatrix} \Psi_1^{(r)} & \Psi_2^{(r)} & B_{w(r)}(\delta) & \tilde{\mathbf{C}}'_{(r)} \\ * & -\mu(\mathcal{Z}_{(r)} + \mathcal{Z}'_{(r)}) & \mu B_{w(r)}(\delta) & \mathbf{0} \\ * & * & -\gamma \mathbf{I} & \mathbf{D}'_{wz} \\ * & * & * & -\gamma \mathbf{I} \end{bmatrix} < 0. \quad (45)$$

#### 4.2 D-stability Region via LMIs

The closed-loop poles of system (34) are constrained to a region  $\mathcal{D}$  of the complex plane if there exists  $\mathbf{P}^{(r)}(\delta) > 0$ , such that (Chilali and Gahinet, 1996)

$$\mathbf{L}_1 \otimes \mathbf{P}^{(r)}(\delta) + \mathbf{L}_2 \otimes (\mathbf{A}^{(r)}(\delta) + \mathbf{B}_u^{(r)}(\delta)\mathbf{K}_{(r)}(\delta))\mathbf{P}^{(r)}(\delta) + \mathbf{L}'_2 \otimes (\mathbf{P}^{(r)}(\delta))'(\mathbf{A}^{(r)}(\delta) + \mathbf{B}_u^{(r)}(\delta)\mathbf{K}_{(r)}(\delta))' < 0, \quad (46)$$

where  $\mathbf{L}_1$  and  $\mathbf{L}_2$  are matrices that shape the  $\mathcal{D}$ -region.

The development in this section is limited for the particular case in which the poles of the closed-loop system are constrained in a circle of radius  $r_a \in \mathbb{R}$ , centered at  $c \in \mathbb{R}$  of the complex plane. This region is determined by the matrices

$$\mathbf{L}_1 = \begin{bmatrix} -r_a & c \\ c & -r_a \end{bmatrix}, \quad \mathbf{L}_2 = \begin{bmatrix} 0 & 1 \\ 0 & 0 \end{bmatrix}. \quad (47)$$

Accordingly, by replacing (47) in (46), performing a congruent transformation considering the matrix

$$\Theta \triangleq \begin{bmatrix} (\mathcal{Z}_{(r)})'(\mathbf{P}^{(r)}(\delta))^{-1} & \mathbf{0} \\ * & (\mathcal{Z}_{(r)})'(\mathbf{P}^{(r)}(\delta))^{-1} \end{bmatrix}, \quad (48)$$

and considering the same change of variables used in the previous subsection, one obtains

$$\Gamma^{(r)} = \begin{bmatrix} -r_a \mathbf{P}^{(r)}(\delta) & \Psi_3^{(r)} \\ * & -r_a(\mathcal{Z}_{(r)} + (\mathcal{Z}_{(r)})' - \mathbf{P}^{(r)}(\delta)) \end{bmatrix} < 0. \quad (49)$$

with,  $\Psi_3^{(r)} = c\mathcal{Z}_{(r)} + \mathbf{A}^{(r)}(\delta)\mathcal{Z}_{(r)} + \mathbf{B}_u^{(r)}(\delta)\mathcal{Y}_{(r)}(\delta)$ .

#### 4.3 Optimization Problem

To cope with the double convex combination sum that appears in both  $\Psi_1^{(r)}$  and  $\Psi_2^{(r)}$  in equation (45) and  $\Psi_3^{(r)}$  in equation (49), the following Lemma is employed,

*Lemma 2.* (Adapted from Wang and Tanaka (2004)) Considering  $\sum_{i=1}^{n_k} \delta^{(i)}(u_{b_{tr}}) \sum_{j=1}^{n_k} \delta^{(j)}(u_{b_{tr}}) G_{ij} < 0, \forall i, j \in \{1, 2, \dots, n_k\}$  where  $n_k$  is the number of vertex systems that

compose equation (34), a sufficient condition is presented by

$$G_{ii} < 0, \quad (50)$$

$$G_{ij} + G_{ji} < 0, \quad j > i. \quad (51)$$

Thus, considering the pole clustering LMI (49), the  $\mathcal{H}_\infty$  candidate controllers can be designed by solving

$$\begin{aligned} & \min_{\mathcal{Z}_{(r)}, \mathcal{Y}_{(r)}(\delta), \mathbf{P}^{(r)}(\delta)} \gamma, \\ \text{s.t. } & \mathbf{P}^{(r)}(\delta) > 0, \quad \Psi_{ii}^{(r)} < 0, \quad \Gamma_{ii}^{(r)} < 0, \\ & \Psi_{ij}^{(r)} + \Psi_{ji}^{(r)} < 0, \quad j > i, \quad \Gamma_{ij}^{(r)} + \Gamma_{ji}^{(r)} < 0, \quad j > i. \end{aligned} \quad (52)$$

#### 4.4 Adaptive Mixing Control Law

The mixing scheme is performed within the subsets intersection by a convex combination of all candidate controllers given by

$$\Delta \mathbf{u}(t) = \mathbf{K}_\infty \Delta \mathbf{x}(t), \quad (53)$$

with

$$\begin{aligned} \mathbf{K}_\infty = & \left( \sum_{r=1}^{n_r} \eta^{(r)}(u_{b_{tr}}(t)) \sum_{k=1}^{n_k} \delta^{(k)}(u_{b_{tr}}(t)) \mathcal{Y}_{(k)} \right) \\ & \times \left( \sum_{r=1}^{n_r} \eta^{(r)}(u_{b_{tr}}(t)) \mathcal{Z}_{(r)} \right)^{-1}. \end{aligned} \quad (54)$$

The mixing signals,  $\eta^{(r)}(u_{b_{tr}}(t))$ , determine the contribution of each candidate controller in the final control law (53), according to the magnitude of the desired convertible UAV forward velocity  $u_{b_{tr}}(t)$ . These signals obey the following properties: i)  $\sum_{r=1}^{n_r} \eta^{(r)}(u_b(t)) = 1$ ; ii)  $\eta^{(r)}(u_b(t)) = 0$  if  $u_{b_{tr}}(t) \notin {}^{(r)}\Omega$ ; and iii)  $\eta^{(r)}(u_{b_{tr}}(t)) \geq 0$ . They are computed as

$$\eta^{(r)}(u_{b_{tr}}) = \chi^{(r)} \left( \frac{u_{b_{tr}} - \bar{a}^{(r)}}{\bar{b}^{(r)}} \right) / \sum_{r=1}^{n_r} \chi^{(r)} \left( \frac{u_{b_{tr}} - \bar{a}^{(r)}}{\bar{b}^{(r)}} \right), \quad (55)$$

using the bump function

$$\chi^{(j)}(\cdot) = \begin{cases} e^{(-1/(1-(\cdot)^2))}, & \text{if } |(\cdot)| < 1, \\ 0, & \text{otherwise,} \end{cases} \quad (56)$$

where  $\bar{a}^{(r)} = \frac{{}^{(r)}u_{b_{tr}}^{max} + {}^{(r)}u_{b_{tr}}^{min}}{2}$  and  $\bar{b}^{(r)} = \frac{{}^{(r)}u_{b_{tr}}^{max} - {}^{(r)}u_{b_{tr}}^{min}}{2}$  are the respective center and cut off values of the subset  ${}^{(r)}\Omega$ . The stability proof of the closed-loop system (32) with the control law (53) follows similarly to the proof of the adaptive mixing controller proposed in Cardoso et al. (2021).

## 5. HARDWARE IN THE LOOP EXPERIMENTS

The numerical experiment was conducted in a general purpose desktop computer running Ubuntu, version 20.04, with the ProVANT Simulator. The ProVANT simulator<sup>4</sup> is a software developed at Federal University of Minas Gerais (UFMG) and released under the MIT open-source license. This software was created on Gazebo and Robotic Operating System (ROS) with the primary goal of providing high-fidelity simulations with visual feedback of control strategies designed for UAVs. To execute the simulator, Gazebo was configured to use the Open Dynamics Engine

<sup>4</sup> The ProVANT simulator software is available for download on <https://github.com/Guiraffo/ProVANT-Simulator>.

(ODE), taking into consideration a time step of 4ms and a sample time of 12ms for the controller. The control law was executed in a raspberry Pi 4 model B SBS with a quadcore ARM Cortex-A72 processor running at 1.5 GHz, with 8GB of DDR4 RAM and a VideoCore XI GPU. The HIL framework is illustrated in Figure 2<sup>5</sup>.

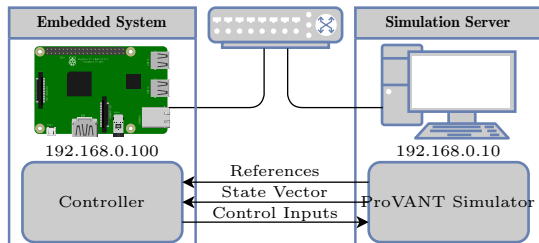


Figure 2. HIL Framework.

In the numerical experiments, the UAV is designated to track a desired trajectory composed of five different stretches, as illustrated in Figure 3. In the first stretch, the UAV takes off from a ground base accelerating forward. At this phase, the aircraft must transition from helicopter flight mode to cruise flight mode. In the second stretch, the UAV reaches cruise speed and performs forward flight. In the third stretch, the UAV is required to perform a circular path, projected in the  $\vec{x}-\vec{y}$  plane, with constant velocity. Since the controller is designed to accomplish forward flight, this phase of the trajectory generates disturbances from unmodeled dynamics, which must be attenuated by the controllers. In the fourth and fifth stretches, the UAV performs the forward flight again but decelerating, then it transitions from cruise to helicopter flight modes, and lands at the final destination.

In order to design the RAMC for the QuadCP-VTOL UAV, the forward velocity,  $u_{b_{tr}}$  ( $\text{m s}^{-1}$ ), was assumed to belong to the range  $\Omega = [0, 48]$  (see (31)). Then, the nonlinear system (28) was trimmed for  $u_{b_{tr}}^{(j)} \in \Omega$  in order to generate the trimming points  $(\vec{x}_{tr}^{(j)}, \mathbf{u}_{tr}^{(j)})$ , for  $j \in \{1, 2, \dots, 49\}$ . The nonlinear system (28) was linearized, augmented with integral actions according to (30), and evaluated in each trimming point  $j$ . Then, the set  $\Omega$  was split into seven subsets according to the properties  $P1)$ ,  $P2)$  and  $P3)$ , such that  $(1)\Omega = [0, 16]$ ,  $(2)\Omega = [12, 22]$ ,  $(3)\Omega = [18, 28]$ ,  $(4)\Omega = [24, 34]$ ,  $(5)\Omega = [30, 40]$ ,  $(6)\Omega = [36, 44]$  and  $(7)\Omega = [40, 48]$ . After, the LPV system (32) was obtained for each subset  $(r)\Omega$ , for  $r \in \{1, 2, \dots, 7\}$  and represented by (33), and the candidate  $\mathcal{H}_\infty$  controllers were generated by solving the convex optimization problem with LMI constraints (52). Accordingly, since the robust adaptive controller is designed to control the altitude and attitude, the outer-loop kinematic controller, presented in Cardoso et al. (2021), is implemented into a cascade structure in order to perform trajectory tracking of the  $x$ - $y$  motion.

In addition, the proposed controller was compared with the mixed  $\mathcal{H}_2/\mathcal{H}_\infty$  controller developed in our previous work (Campos et al., 2021). Since this controller

<sup>5</sup> A video recording of the experiments is available in [https://youtu.be/C6NAAt-Rn\\_T0](https://youtu.be/C6NAAt-Rn_T0).

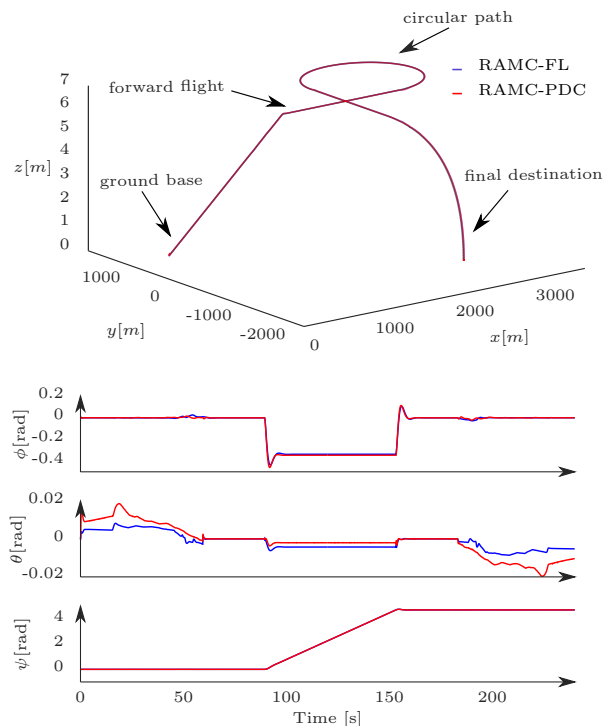


Figure 3. Trajectory Tracking and Orientation.

considers a fixed Lyapunov function, i.e. time invariant, it will be called from now on RAMC-FL, while the controller proposed in this work RAMC-PDC. To perform a fair comparison, both controllers were tuned such that the tracking accuracy, evaluated here through the Integral of the Square Error (ISE) performance index, is similar,  $ISE = \int_0^t (\Delta \mathbf{x})' \Delta \mathbf{x} d\tau$ . The resulted ISE was  $ISE = 1.3908 \cdot 10^9$  for the RAMC-FL against a  $ISE = 1.3907 \cdot 10^9$  for the proposed RAMC-PDC. Also, the control effort was evaluated through the Integral of the Absolute Derivative the Control inPUt (IADU) performance index,  $IADU = \int_0^t \sum_{n=1}^{11} |\frac{du_n(\tau)}{d\tau}| d\tau$ , where  $u_n$  stands for the  $n$ -th element of the input vector, resulting in  $IADU = 2708.9(100\%)$  for RAMC-FL against  $IADU = 1273.5(47.01\%)$  for RAMC-PDC. Hence, it is possible to observe that the controller improved significantly the control effort. The average time and the worst execution time of the RAMC-PDC controller were, respectively,  $T_{average} = 1.1ms$  and  $T_{worst} = 9.9ms$ .

The results of the numerical experiments are shown in Figures 3-5. As can be observed in Figure 3, the controller was able to perform the desired trajectory and reach the final destination. The UAV was able to transit from the helicopter to the airplane flight mode, and vice versa. Also, note that when the QuadCP-VTOL UAV is tracking the circular path, the rolling angle decreases in order to physically provide the capability to fly in a curve. From Figures 3 and 5, one can observe that all the control inputs remained bounded and under feasible values.

## 6. CONCLUSION

This paper designed a RAMC for full-flight envelope trajectory tracking of a QuadCP-VTOL UAV addressing the transition between flight modes problem. An LPV model was obtained from the nonlinear model, candidate linear

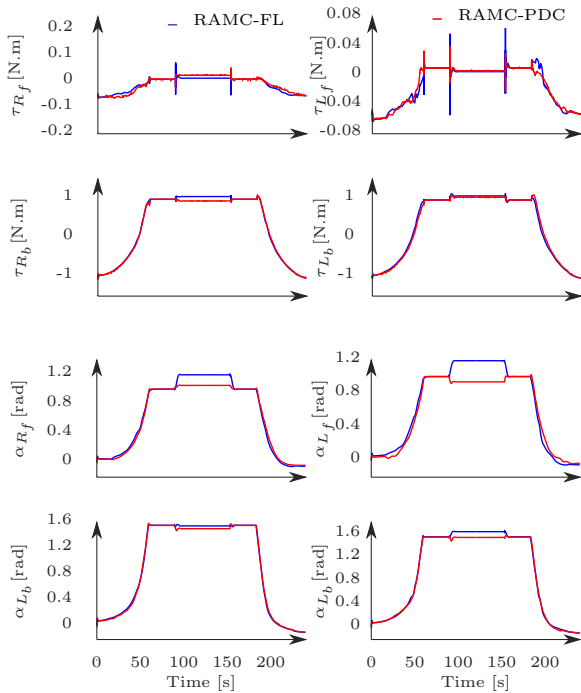


Figure 4. Torques and Thruster Groups Deflection.

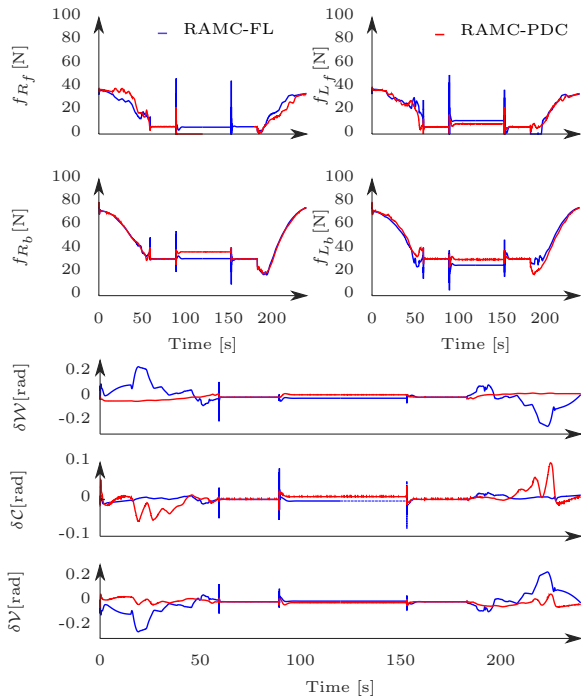


Figure 5. Forces and Aerodynamic Surfaces Deflections.

$\mathcal{H}_\infty$  controllers were designed based on a PDC framework, and an adaptive mixing scheme was implemented to perform a convex combination of the candidate controllers with ensured stability. The efficiency of the proposed control strategy was corroborated with numerical experiments conducted in a HIL framework, and the proposed RAMC-PDC controller was compared with the one in Campos et al. (2021). Both controllers were tuned to achieve the same ISE index, revealing that the proposed RAMC-PDC provides less control effort expenditure which is evidenced

by the IADU index. As future works, we intend to test the proposed RAMC-PDC under the influence of several external disturbances such as environmental wind and wind gusts. In addition, we are going to reformulate the RAMC-PDC considering the time derivative of the UAV forward velocity.

## REFERENCES

- Allenspach, M. and Ducard, G.J.J. (2021). Nonlinear model predictive control and guidance for a propeller-tilting hybrid unmanned air vehicle. *Automatica*, 132, 1–10.
- Baranyi, P. (2004). Tp model transformation as a way to lmi-based controller design. *IEEE TIE*, 51(2), 387–400.
- Campos, J.M., Cardoso, D.N., and Raffo, G.V. (2021). Modeling and robust control for full-flight envelope trajectory tracking of a QuadCP-VTOL unmanned aerial vehicle. In *77th VFS A. Forum & Technology*, 1–17.
- Cardoso, D.N., Esteban, S., and Raffo, G.V. (2021). A new robust adaptive mixing control for trajectory tracking with improved forward flight of a tilt-rotor uav. *ISA transactions*, 110, 86–104.
- Chilali, M. and Gahinet, P. (1996).  $\mathcal{H}_\infty$  design with pole placement constraints: an LMI approach. *IEEE Transactions on Automatic Control*, 41(3), 358–367.
- De Oliveira, M.C., Geromel, J.C., and Bernussou, J. (2002). Extended  $h_2$  and  $h_\infty$  norm characterizations and controller parametrizations for discrete-time systems. *International Journal of Control*, 75(9), 666–679.
- De Oliveira, M.C. and Skelton, R.E. (2001). Stability tests for constrained linear systems. In *Perspectives in robust control*, 241–257. Springer.
- Ducard, G.J. and Allenspach, M. (2021). Review of designs and flight control techniques of hybrid and convertible VTOL UAVs. *Aerospace Science and Technology*, 1–25.
- Hegde, N.T., Vaz, A.C., and Nayak, C. (2021). Closed loop performance analysis of classical PID and robust H-infinity controller for VTOL unmanned quad tiltrotor aerial vehicle. *International Journal of Mechanics*, 15, 211–222.
- Houari, A., Bachir, I., Mohamed, D.K., and Karimohamed, M. (2020). PID vs LQR controller for tilt rotor airplane. *IJECE*, 10(6), 6309–6318.
- Lombaerts, T., Kaneshige, J., Schuet, S., Hardy, G., Aponso, B.L., and Shish, K.H. (2019). Nonlinear dynamic inversion based attitude control for a hovering quad tiltrotor eVTOL vehicle. In *AIAA Scitech 2019 Forum*, 1–26.
- Raffo, G.V., Ortega, M.G., and Rubio, F.R. (2011). Nonlinear  $\mathcal{H}_\infty$  controller for the quad-rotor helicopter with input coupling. *IFAC World Congress*, 44(1), 13834–13839.
- Vendrichoski, J.C., Costa, T.L., ElYoussef, E.S., and de Pieri, E.R. (2019). Mathematical modeling and control of a quadrotor aerial vehicle with tiltrotors aimed for interaction tasks. In *2019 19th ICAR*, 161–166. IEEE.
- Wang, H.O. and Tanaka, K. (2004). *Fuzzy control systems design and analysis: A linear matrix inequality approach*. John Wiley & Sons.
- Willis, J., Johnson, J., and Beard, R.W. (2020). State-dependent lqr control for a tilt-rotor uav. In *2020 ACC*, 4175–4181. IEEE.